CFA-13 – a bifunctional perfluorinated metal–organic framework featuring active Cu(I) and Cu(II) sites†

J. Fritzsche, D. Denysenko, M. Grzywa and D. Volkmer *

The synthesis and crystal structure of the mixed-valent perfluorinated metal–organic framework **(Me_2NH_2)[CFA-13]** (Coordination Framework Augsburg University-13), $(Me_2NH_2)[Cu^{I}_3Cu^{II}_2(tfpc)_4]$ (H_2-tfpc = 3,5-bis(trifluoromethyl)-1*H*-pyrazole-4-carboxylic acid) is described. The copper-containing MOF crystallizes in the monoclinic crystal system within the space group $P2_1/n$ (no. 14) and the unit cell parameters are as follows: a = 22.3887(19), b = 13.6888(8), c = 21.1804(13) Å, β = 90.495(3)°, V = 6491.0(8) Å^3. **(Me_2NH_2)[CFA-13]** features a porous 3-D structure constructed from two types of secondary building units (SBUs). Besides novel trinuclear $[Cu^{I}_3(pz)_4]^-$ coordination units, the network also exhibits Cu(II) paddle-wheel SBUs. **(Me_2NH_2)[CFA-13]** is fully characterized by single crystal X-ray diffraction, thermogravimetric analysis, variable temperature powder X-ray diffraction, IR spectroscopy, photoluminescence, gas sorption measurements and pulse chemisorption experiments. **M[CFA-13]** (M = K^+, Cs^+) frameworks were prepared by postsynthetic exchange of interchannel dimethylammonium cations. Moreover, it was shown that CO molecules can be selectively bound at Cu(I) sites of $[Cu^{I}_3(pz)_4]^-$ units, whereas Cu(II) paddle-wheel units bind selectively NH_3 molecules.

Introduction

Depending on the functionality of the organic ligand, metal–organic frameworks (MOFs) often include preferred secondary building units (SBUs) with corresponding metal ions. The combination of pyrazolate (pz) based ligands with copper ions often leads to the formation of polynuclear SBUs, as for example trinuclear planar $[Cu^{I}_3(pz)_3]$ units,[1] while carboxylate-based linkers favor to build up Cu(II) paddle-wheel SBUs within a MOF structure.[2] Compounds containing $[Cu^{I}_3(pz)_3]$ SBUs are of particular interest for oxygen activation and redox catalysis[3] because of their structural and functional relation to catalytically active sites present in natural enzymes (*e.g.* oxidases and oxygenases). Furthermore, such compounds are used as luminescent sensors or in phosphorescence-emitting devices.[4] Moreover, MOFs containing polynuclear $[Cu^{I}_n(pz)_m]$ SBUs often show strong binding of small gas molecules as for example carbon monoxide[5] as well as selective and rapid sorption of hydrocarbons over water.[6]

The most famous MOF containing Cu(II) paddle-wheel units is HKUST-1, which was first synthesized in 1999.[7] Until today many research groups work with this compound and it finds a constantly expanding field of applications. Besides gas storage[8] and separation,[9] HKUST-1 is utilized in sensor technology,[10] catalysis[11] as well as in electrical conductivity applications.[12] Within the structure of HKUST-1 two antiferromagnetically coupled Cu(II) ions are coordinated by four carboxylate groups of 1,3,5-benzenetricarboxylate ligands. Additionally, two water molecules are weakly bound in axial positions at the Cu(II) centres. Removal of the coordinated solvent molecules by heating the MOF in vacuum leads to free accessible, unsaturated and highly reactive Lewis acidic copper sites. These well-defined Cu(II) species show quite strong chemisorption of small basic gas molecules as for example ammonia with an isosteric heat of adsorption of 60 kJ mol^{-1}.[8,13] This makes HKUST-1 very interesting for potential application in biogas waste filtration.[8,14] In contrast, carbon monoxide, which typically binds strongly at Cu(I) sites, does not show chemisorption at Cu(II) paddle-wheel units, as shown by its low isosteric heat of adsorption (17 kJ mol^{-1}) in HKUST-1.[15]

In this paper we present the novel mixed-valent perfluorinated MOFs **(Me_2NH_2)[CFA-13]** and **M[CFA-13]** (M = K^+, Cs^+),

Augsburg University, Institute of Physics, Chair of Solid State and Materials Chemistry, Universitaetsstrasse 1, 86159 Augsburg, Germany.
E-mail: dirk.volkmer@physik.uni-augsburg.de; Fax: +49 (0)821 598 5955; Tel: +49 (0)821 598 3006

†Electronic supplementary information (ESI) available: Crystallographic and EDX data; XRPD patterns; IR spectra; TGA, gas sorption and pulse chemisorption measurements. CCDC 1559842. For ESI and crystallographic data in CIF or other electronic format see DOI: 10.1039/c7dt02512b

which are build up from the bifunctional linker 3,5-bis(trifluoromethyl)-1*H*-pyrazole-4-carboxylic acid (H_2-tfpc) and therefore contain both trinuclear $[Cu^{I}_3(pz)_4]^-$ and Cu(II) paddle-wheel SBUs within one structure. The crystal structure of **(Me_2NH_2)[CFA-13]** was determined by single crystal X-ray structure analysis. In addition, **(Me_2NH_2)[CFA-13]** was characterized by thermogravimetric analysis, variable temperature X-ray diffraction, IR spectroscopy, photoluminescence, gas sorption measurements and pulse chemisorption experiments. Moreover, chemisorption properties of **(Me_2NH_2)[CFA-13]** towards CO and NH_3 molecules were investigated.

Results and discussion

Syntheses and characterization

3,5-Bis(trifluoromethyl)-1*H*-pyrazole-4-carboxylic acid (H_2-tfpc) was synthesized according to literature procedure.[16]

(Me_2NH_2)[CFA-13] framework was obtained as cyan block crystals (see Fig. 1a and b) after heating a DMF solution of H_2-tfpc and copper(II) nitrate trihydrate at 120 °C (Scheme 1). The freshly prepared sample contains DMF molecules in the crystal structure. These DMF molecules can be exchanged with different other solvents by Soxhlet extraction. The final products are labelled as **(Me_2NH_2)[CFA-13](solvent)**, where the solvent in the brackets refers to DMF, CH_2Cl_2, EtOH, MeOH, acetone or THF. The solvents used for exchange show different polarity increasing in the following order: CH_2Cl_2 < THF < acetone < EtOH < MeOH. In this row, MeOH and EtOH are highly polar protic and hydrophilic, acetone and THF polar aprotic solvents, whereas CH_2Cl_2 is a non-polar solvent. Due to different boiling points and polarity the solvents have great influence on crystal stability, activation as well as physical and chemical properties. The colour of the samples changes from cyan (DMF, CH_2Cl_2, acetone, THF) to green (MeOH, EtOH) according to the included solvent molecules, which is related to changing coordination environment of Cu(II) paddle-wheel units (see Fig. 1c and d).

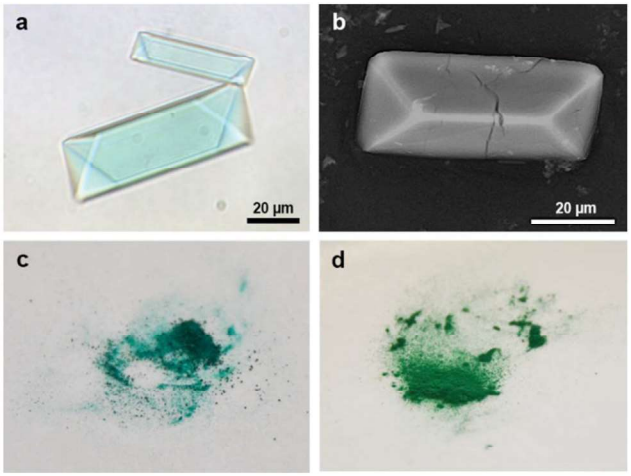

Fig. 1 (a) Optical micrograph and (b) SEM image of **(Me_2NH_2)[CFA-13]**; (c) powder sample of **(Me_2NH_2)[CFA-13](DMF)**; (d) powder sample of **(Me_2NH_2)[CFA-13](MeOH)**.

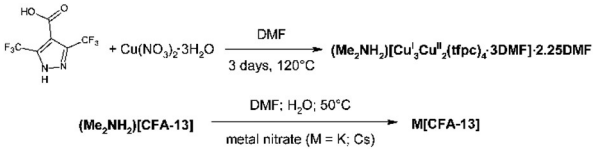

Scheme 1 Synthesis of **(Me_2NH_2)[CFA-13]** and **M[CFA-13]** (DMF = *N*,*N*-dimethylformamide).

Substituted **M[CFA-13]** frameworks (M^+ = K^+, Cs^+) were obtained *via* postsynthetic cation exchange upon treatment of **(Me_2NH_2)[CFA-13]** with a solution of the corresponding metal nitrate in a DMF/H_2O mixture at 50 °C. The detailed exchange procedure is given in the Experimental section. The molar ratios of Cu/M in the obtained products were determined by energy dispersive X-ray spectroscopy (EDX) and correspond well to the expected theoretical values (5 : 1 for singly charged cations K^+ and Cs^+, see ESI, Fig. S15 and S16 and Table S2†). XRPD patterns of exchanged **M[CFA-13]** frameworks show similar peak positions as **(Me_2NH_2)[CFA-13]** (see ESI, Fig. S14†).

Single crystal structure analysis of $(Me_2NH_2)[Cu^{I}_3Cu^{II}_2(tfpc)_4{\cdot}3DMF]{\cdot}2.25DMF$

Single crystal X-ray diffraction studies reveal that **$(Me_2NH_2)[Cu^{I}_3Cu^{II}_2(tfpc)_4{\cdot}3DMF]{\cdot}2.25DMF$** crystallizes in the monoclinic crystal system within the space group $P2_1/n$ (no. 14). The asymmetric unit consists of five copper atoms, four $tfpc^{2-}$ ligands, five DMF molecules and one $Me_2NH_2^+$ cation. Three DMF molecules are coordinated to the copper centres, another two DMF molecules as well as a dimethylammonium cation are filling the pores of the framework. An ORTEP-style plot of the asymmetric unit and a detailed description of the crystal structure of **$(Me_2NH_2)[Cu^{I}_3Cu^{II}_2(tfpc)_4{\cdot}3DMF]{\cdot}2.25DMF$** are presented in the ESI (Fig. S17 and Tables S3–S6†).

$(Me_2NH_2)[Cu^{I}_3Cu^{II}_2(tfpc)_4{\cdot}3DMF]{\cdot}2.25DMF$ features a 3-D non-interpenetrated microporous structure constructed from trinuclear $[Cu^{I}_3(pz)_4]^-$ and paddle-wheel $[Cu^{II}_2(O_2C)_4]$ secondary building units, expanding alternately in 3-dimentions (see Fig. 2a–c). Two Cu(I) ions within the trinuclear SBU are three-fold coordinated in a trigonal planar arrangement by pyrazolate N-donor atoms from the ligand molecules while the third Cu(I) ion is coordinated by two N-donor atoms from the ligand molecules in a nearly linear arrangement. This Cu(I)-ion is additionally coordinated in 'T-type' mode by one oxygen atom from the weakly bonded DMF molecule (Cu^{I}–O_{DMF} = 2.46 Å). The Cu–N distances range from 1.955(4)–2.024(5) Å for the tree-fold coordinated Cu(I)-ions, compared to 1.911(4)–1.914(2) Å for the linear coordinated Cu(I). These values are in good agreement with those found in structurally related Cu-MOFs.[17] Two $tfpc^{2-}$ ligands of the trinuclear $[Cu^{I}_3(pz)_4]^-$ SBU, bound to linear coordinated Cu(I) ions, are located in the same plane with three Cu(I) ions, whereas the two remaining $tfpc^{2-}$

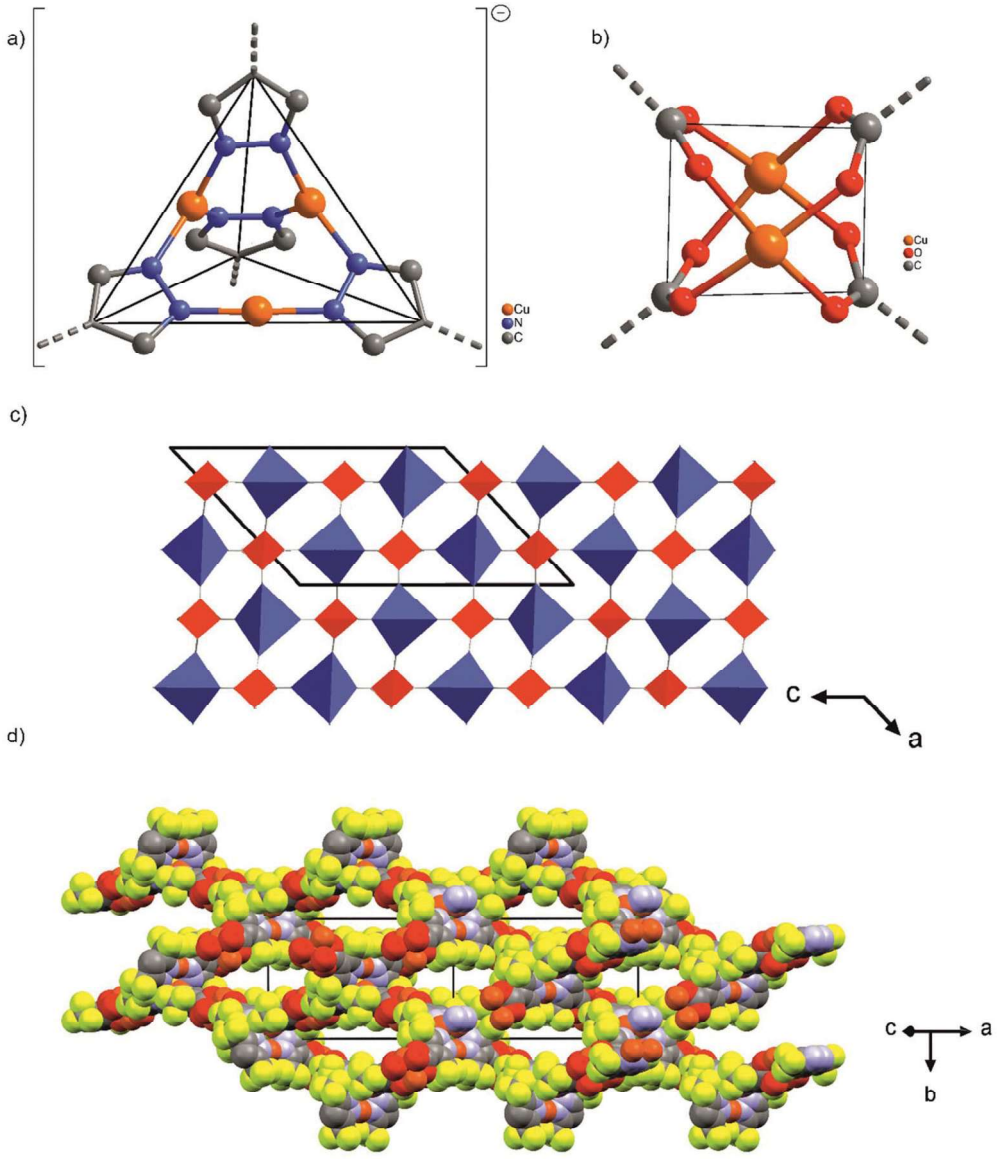

Fig. 2 (a) Coordination unit of the $(Me_2NH_2)[Cu^{I}_3Cu^{II}_2(tfpc)_4\cdot 3DMF]\cdot 2.25DMF$ framework featuring trinuclear Cu(I) moieties. CF_3-groups have been omitted for clarity; (b) paddle-wheel coordination unit of the $(Me_2NH_2)[Cu^{I}_3Cu^{II}_2(tfpc)_4\cdot 3DMF]\cdot 2.25DMF$ framework featuring dinuclear Cu(II) moieties; (c) schematic packing diagram representing SBUs of $(Me_2NH_2)[Cu^{I}_3Cu^{II}_2(tfpc)_4\cdot 3DMF]\cdot 2.25DMF$, viewed in *b*-direction; (d) portion of the crystal structure of $(Me_2NH_2)[Cu^{I}_3Cu^{II}_2(tfpc)_4\cdot 3DMF]\cdot 2.25DMF$ emphasizing pores, viewed in [101] direction. DMF molecules and dimethylamine cations were omitted for clarity.

ligands, bridging trigonal planar coordinated Cu(I) ions, are located above and below the trigonal planar Cu^{I}_3 array. The mixed-valent complex $[Cu(II)_2Cu(I)(F_6dmpz)_5]$ (F_6dmpzH = 3,5-bis(trifluoromethyl)pyrazole) contains similar trinuclear Cu_3-pyrazolate units, where two Cu(II) ions are bridged by two additional pyrazolate ligands above and below the trigonal $[Cu_3(pz)_3]$ plane.[18] To the best of our knowledge, **(Me_2NH_2)[CFA-13]** represents a first example of $[Cu^{I}_3(pz)_4]^-$ coordination units.

The coordination sphere of the Cu(II) ions in the paddle-wheel SBU could be considered pseudooctahedral, assuming four oxygen atoms from four $tfpc^{2-}$ ligands in equatorial plane and one oxygen atom from a coordinated DMF molecule and the second Cu(II) ion from the paddle-wheel dimer in the apical positions. The Cu^{II}–Cu^{II} distance in the paddle-wheel SBU is equal to 2.6270(9) Å. This value is in good agreement with those found in structurally related Cu-MOFs.[19] Compared to a trinuclear Cu(I)-containing SBU, the coordination of DMF molecules at Cu(II) paddle-wheel units is considerably stronger, as indicated by shorter Cu^{II}–O_{DMF} distance of 2.126 Å.

The SBUs of **$(Me_2NH_2)[Cu^{I}_3Cu^{II}_2(tfpc)_4\cdot 3DMF]\cdot 2.25DMF$** are connected by single C–C bonds and create pores expanding in the [101] direction of the crystal lattice (see Fig. 2d). Taking the van der Waals radii of fluorine atoms (1.35 Å) into account,

the limiting pore diameter calculated between the fluorine atoms of the CF_3-groups is 3.07 Å. Estimation with the program SQUEEZE[20] for the structure of **CFA-13** without non-coordinated DMF reveals an initial solvent accessible void volume of 2454.3 $Å^3$ (0.274 $cm^3\ g^{-1}$), which is 37.8% of the unit cell volume (6491.0(7) $Å^3$) for a probe radius of 2.07 Å,[21] corresponding to the approximate van der Waals radius of carbon dioxide. In the crystal structure of **$(Me_2NH_2)[Cu^I_3Cu^{II}_2(tfpc)_4]\cdot 3DMF]\cdot 2.25DMF$** the pores are occupied by DMF molecules and dimethylammonium cations which compensate a negative charge of the lattice. These dimethylammonium cations can be readily exchanged by alkaline metal ions, as described in detail in the synthesis part and Experimental section. The lattice DMF molecules are disordered. Between both equivalent disordered DMF ligands was found additional electron density which was assigned to 0.25 independent DMF molecule (one molecule per unit cell).

Thermal analysis and VTXRPD studies

Thermal and structural stability of **(Me_2NH_2)[CFA-13]** samples containing different solvent molecules was determined by TGA and VTXRPD measurements. As shown in Fig. 3 and ESI (Fig. S8 and S9†), the thermogravimetric profile under nitrogen of as-synthesized **(Me_2NH_2)[CFA-13](DMF)** (black line) exhibits two weight loss steps. In the temperature range of 50–150 °C, the weight loss (9.3%) is attributed to the removal of DMF molecules from the pores. The further weight loss above 180 °C is due to the decomposition of the MOF and formation of CuO as the final product. Since the TGA profile of **(Me_2NH_2)[CFA-13](DMF)** reveals no clear plateau range, suitable for solvent removal, thermal stability of solvent-exchanged **(Me_2NH_2)[CFA-13]** samples was further investigated. TGA measurements have shown that the samples obtained after exchange with MeOH, EtOH and CH_2Cl_2 and pre-heated at 150 °C show a stable plateau range up to 200 °C (see ESI Fig. S10†). The THF-exchanged sample shows weight loss already above 150 °C, which could be due to the presence of small amounts of coordinated DMF molecules. Details about the characterization of solvent-exchanged **(Me_2NH_2)[CFA-13]** samples are given in ESI (sections 2 and 3 and Fig. S8–S12†).

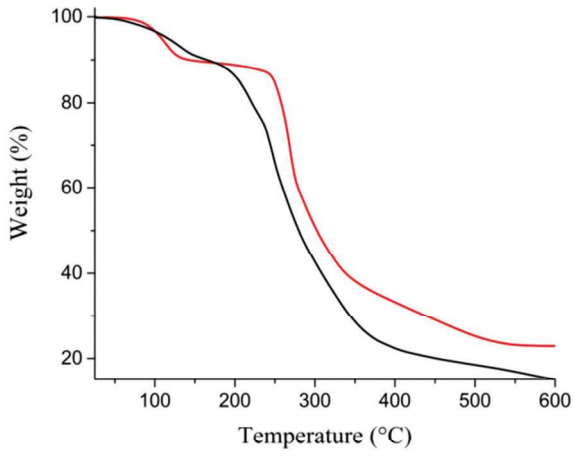

Fig. 3 Temperature dependent weight loss of **(Me_2NH_2)[CFA-13](DMF)** (black) and **K[CFA-13](DMF)** (red) under flowing nitrogen gas.

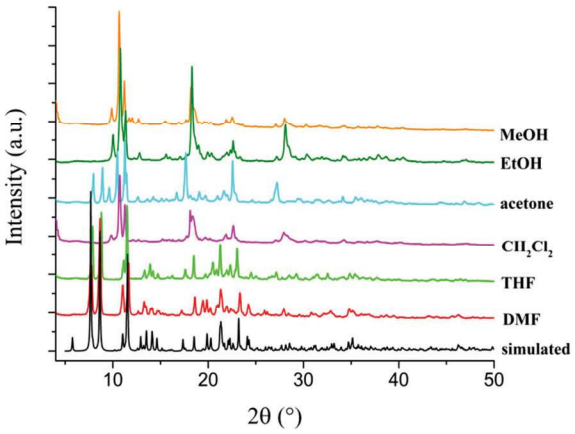

Fig. 4 XRPD plots of **(Me_2NH_2)[CFA-13]** with different included solvents. The black XRPD pattern is simulated based on single crystal X-ray data of **$(Me_2NH_2)[Cu^I_3Cu^{II}_2(tfpc)_4\cdot 3DMF]\cdot 2.25DMF$**.

Compared to **(Me_2NH_2)[CFA-13](DMF)** the TGA curve of **K[CFA-13](DMF)** (Fig. 3, red line) shows a more pronounced weight plateau between 150–220 °C indicating that no solvent molecules are coordinated to K^+ ions. Such behavior can be explained by very weak coordinating properties of K^+ ions. Above 220 °C, the framework starts to decompose.

Phase purity of **(Me_2NH_2)[CFA-13](DMF)** was confirmed by XRPD measurements. The experimental XRPD pattern (Fig. 4, red curve) is consistent with the one calculated from the single crystal structural data (Fig. 4, black curve). Differences in peak intensities are due to occluded solvent molecules. Exchanging the included DMF molecules with other solvents leads to dramatic changes in XRPD pattern due to the high flexibility of the structure. **(Me_2NH_2)[CFA-13](THF)** shows quite similar reflex positions as **(Me_2NH_2)[CFA-13](DMF)**. **(Me_2NH_2)[CFA-13](CH_2Cl_2)** and **(Me_2NH_2)[CFA-13](acetone)** show XRPD patterns related to **(Me_2NH_2)[CFA-13](DMF)**, but the characteristic reflexes below 10° 2θ are slightly shifted to higher 2θ values and become less intensive. Apart from the missing characteristic reflexes below 10° 2θ, MeOH- and EtOH-exchanged samples have similar XRPD patterns as **(Me_2NH_2)[CFA-13](CH_2Cl_2)** and **(Me_2NH_2)[CFA-13](acetone)**. Variable temperature X-ray powder diffraction (VTXRPD) studies of **(Me_2NH_2)[CFA-13](DMF)** (Fig. 5) are in good agreement with the results from the TGA measurements. The framework is stable up to 100 °C. At 150 °C, several new peaks appear while the intensity of the original peaks decreases. Above 200 °C, the decomposition of the compound is observed and Cu (PDF no. 4-836) is formed as a new crystal phase at 400 °C.

Gas sorption measurements

Nitrogen adsorption isotherm for **(Me_2NH_2)[CFA-13](MeOH)** at 77 K reveals only very low BET surface area of <10 $m^2\ g^{-1}$. However, CO_2 sorption isotherms on **(Me_2NH_2)[CFA-13]**

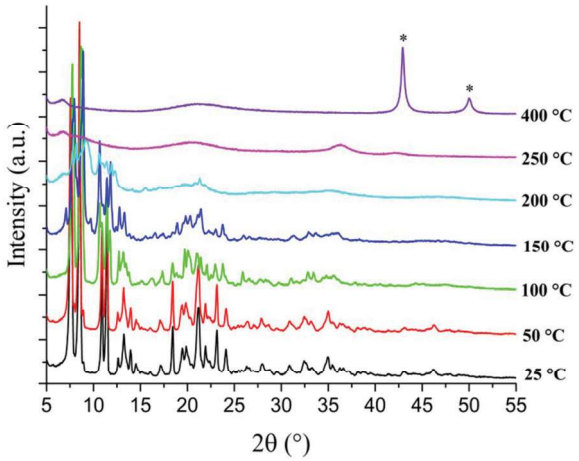

Fig. 5 VTXRPD plots of **(Me$_2$NH$_2$)[CFA-13](DMF)** in the range of 25–400 °C (* – peaks: Cu phase, PDF no. 4-836).

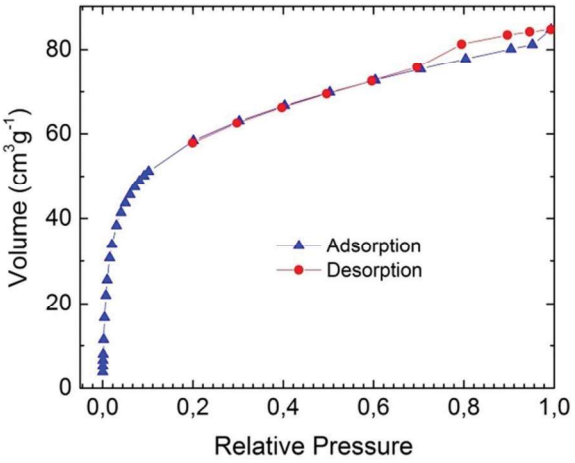

Fig. 6 CO_2 adsorption (blue) and desorption (red) isotherms of **(Me$_2$NH$_2$)[CFA-13](THF)** at 194.7 K.

(CH$_2$Cl$_2$), **(Me$_2$NH$_2$)[CFA-13](MeOH)**, **(Me$_2$NH$_2$)[CFA-13](acetone)**, **(Me$_2$NH$_2$)[CFA-13](DMF)** and **(Me$_2$NH$_2$)[CFA-13](THF)** samples at 273 K up to p/p_0 = 0.03 (see ESI, Fig. S1†) confirm permanent porosity of the frameworks and reveal the BET surface areas of 152, 239, 252, 275 and 298 m^2 g^{-1}, respectively. **K[CFA-13]** shows a similar BET surface of 288 m^2 g^{-1}. Due to its smaller kinetic diameter (3.3 Å) and higher measurement temperature CO_2 can diffuse into the pores of the framework with a very small limiting diameter (3.07 Å, see crystal structure description), whereas N_2, having a larger kinetic diameter (3.64 Å), cannot enter the pores at 77 K. The BET surface area for **(Me$_2$NH$_2$)[CFA-13](CH$_2$Cl$_2$)** is considerably lower as compared to the other samples which might be due to the high flexibility of the structure and strong distortion after exchange with non-polar solvent molecules (as dichloromethane is very volatile and therefore vacates the pores quickly).

Since **(Me$_2$NH$_2$)[CFA-13](THF)** shows the highest BET surface area within the tested row, this sample was chosen for further sorption studies. The CO_2 adsorption/desorption isotherm at 194.7 K follows type I behaviour, which is characteristic for microporous solids (Fig. 6). The maximum uptake achieved at p/p_0 = 0.99 is 84.6 cm^{-3} g^{-1} which corresponds to a total pore volume of 0.11 cm^3 g^{-1}. This value is considerably lower as calculated from the crystal structure data (0.274 cm^3 g^{-1}), which might be related to the structural changes of the framework occurring upon solvent exchange and removal. The slight hysteresis observed in the p/p_0 range of 0.7–1 points at the framework flexibility as well. The BET surface area, determined in the p/p_0 range of 0.04–0.1, is 233 m^2 g^{-1}.

The isosteric heat of CO adsorption for **(Me$_2$NH$_2$)[CFA-13](THF)** determined from adsorption isotherms measured in the temperature range of 213–243 K (see ESI, Fig. S3†) reaches a rather high value of 47 kJ mol^{-1} at low loading (<0.2 mmol g^{-1}) and decreases to typical physisorption values of ~20 kJ mol^{-1} at >0.8 mmol g^{-1} loading (Fig. 7, green curve). Such behavior hints at a weak binding of carbon monoxide to the active

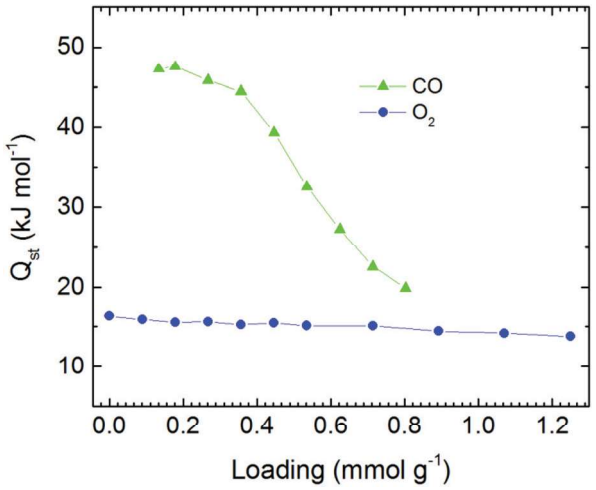

Fig. 7 Dependencies of the isosteric heats of CO (green) and O_2 (blue) adsorption on the loading in **(Me$_2$NH$_2$)[CFA-13](THF)**.

Cu sites of the **CFA-13** framework. The amount of chemisorbed CO molecules roughly estimated from the dependence of the isosteric heat of adsorption on loading (approx. 0.7 mmol g^{-1}) corresponds well to one Cu centre per SBU (0.74 mmol g^{-1}). This stoichiometry and the fact that CO does not show any chemisorption at Cu(II) paddle-wheel units in HKUST-1,[15] speaks for the selective binding of CO molecules at linearly coordinated Cu(I) ions from trinuclear $[Cu^{I}_{3}(pz)_4]^-$ SBUs. These Cu(I) sites were also found to bind weakly to DMF molecules (see crystal structure description). Oxygen adsorption isotherms for **(Me$_2$NH$_2$)[CFA-13](THF)** (see ESI, Fig. S2†) reveal a nearly constant physisorption heat of 14–16 kJ mol^{-1} (Fig. 7, blue curve) and thus oxygen does not bind to the Cu(I) centres.

In addition, the adsorption of CO in **(Me$_2$NH$_2$)[CFA-13](THF)** was further studied by diffuse reflectance Fourier-transform IR spectroscopy (DRIFT) (see Fig. 8). First, the sample

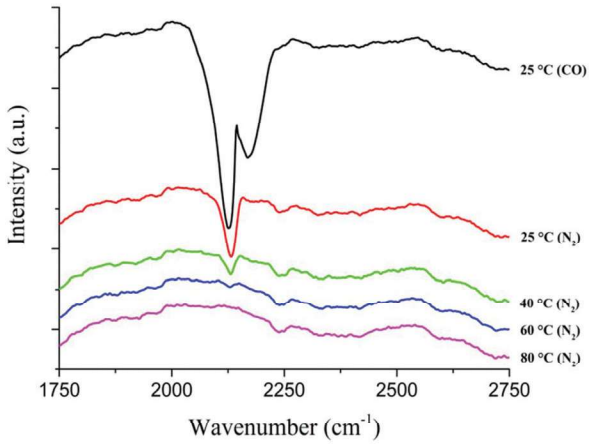

Fig. 8 *In situ* DRIFT spectra of activated **(Me$_2$NH$_2$)[CFA-13](THF)** under CO atmosphere at room temperature and upon subsequent heating up to 80 °C under N_2 atmosphere.

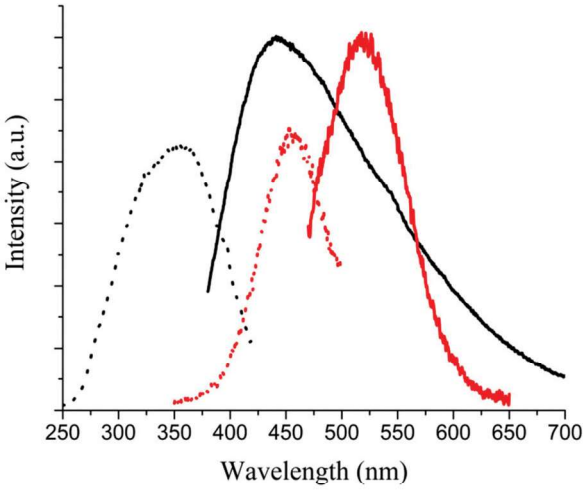

Fig. 9 Solid-state photoluminescence spectra of **(Me$_2$NH$_2$)[CFA-13]** (red) and the **H$_2$-tfpc** ligand (black) at room temperature. Dashed lines: excitation spectra; continuous lines: emission spectra.

was heated up to 100 °C under nitrogen flow. After cooling down to room temperature, an FT-IR spectrum of the activated **(Me$_2$NH$_2$)[CFA-13]** was recorded under nitrogen. Then, the gas flow was switched to CO and another spectrum was recorded. The bands at 2169 cm^{-1} and 2127 cm^{-1} at room temperature (black line) can be assigned to free CO molecules in the gas phase. After a few minutes under CO atmosphere, the gas flow was changed to nitrogen again, followed by the stepwise heating up to 80 °C. A new single band at 2132 cm^{-1} was detected. This band results from CO molecules bound to Cu(I) ions, as already shown by an enhanced isosteric heat of CO adsorption (Fig. 7). The CO binding is quite strong, as the DRIFT-spectrum shows, that the gas molecules remain at least partially bound up to 60 °C. Above this temperature, all CO molecules are removed. The recorded band at 2132 cm^{-1} corresponds to the stretch mode of the CO molecules coordinatively bound to Cu(I) ions and is in good agreement with literature data of Cu(I) pyrazolate complexes (for instance, ν_{CO} = 2137 cm^{-1} for [Cu{HB(3,5-(CF$_3$)$_2$pz)$_3$}(CO)]).[22]

Ammonia pulse chemisorption

To prove the reactivity of the **(Me$_2$NH$_2$)[CFA-13]** framework towards Lewis basic probe molecules, ammonia pulse chemisorption measurements at 100 °C were performed (for details see Experimental section and ESI, Fig. S13†). The amount of chemisorbed NH_3 molecules, determined from these measurements (35.3 ± 2.5 cm^{-3} g^{-1}, or 1.57 ± 0.11 mmol g^{-1}), corresponds well to two Cu centres per SBU (1.48 mmol g^{-1}) and thus confirms selective binding of ammonia at Cu(II) paddle-wheel units with a 1 : 1 Cu(II)/NH_3 stoichiometry.

Photoluminescence and UV-Vis spectroscopy

Solid-state photoluminescence properties of **(Me$_2$NH$_2$)[CFA-13]** and H_2-tfpc ligand were studied at room temperature. H_2-tfpc exhibits a broad emission peak under excitation at 360 nm (Fig. 9, black line) and shows maximum emission at 440 nm. The excitation of H_2-tfpc is probably attributed to the $\pi \rightarrow \pi^*$ transition of the aromatic system. The emission peak of **(Me$_2$NH$_2$)[CFA-13]** (Fig. 9, red line) is red-shifted and shows maximum emission at 520 nm under excitation at 455 nm, while the emission of the ligand disappears. For Cu(I) pyrazolates, the Cu–Cu distance has an extensive influence on the photoluminescent properties of the material. Normally, the Cu–Cu distance must be less than or close to twice the van der Waals radius of Cu(I) (1.4 Å) to achieve a low energy emission. In **CFA-13**, the closest Cu^{I}–Cu^{I} distance is 2.907 Å. This value seems too large to influence the luminescence properties by intramolecular Cu···Cu interactions. We presume that the observed emission is related to a metal-to-ligand charge transfer. Upon irradiation with a blue-violet light, the Cu(I) ions within the trinuclear $[Cu^{I}_3(pz)_4]^-$ units undergo a metal-to-ligand charge transfer resulting in a charge-separated excited singlet state. This state can either decay to the ground state by the emission of slightly red-shifted photons or undergo a spin conversion into an excited triplet state, which shows a slow decay (luminescence) to the ground state.[23] The latter transition might be influenced by weak Cu···Cu interactions that typically occur in Cu(I) complexes and coordination polymers comprising bridging pyrazolate moieties.

The intense green to cyan colour of **(Me$_2$NH$_2$)[CFA-13]** crystals is a first indication for the presence of Cu(II) centres in the framework structure. In order to confirm the coordination environment of copper(II) centres in the paddle-wheel units, **(Me$_2$NH$_2$)[CFA-13](solvent)** (solvents: DMF, acetone, CH_2Cl_2, MeOH or THF) were analysed by solid-state UV-vis spectroscopy. All samples show two strong absorption bands with maxima at 370–390 nm and 715–750 nm with shoulders at approx. 260 nm and 950–960 nm, respectively (Fig. 10). The absorption bands in the range of 370–390 nm can either originate from ligand-to-metal charge transfer from oxygen in the carboxylate to Cu(II) ions or from intraligand electron tran-

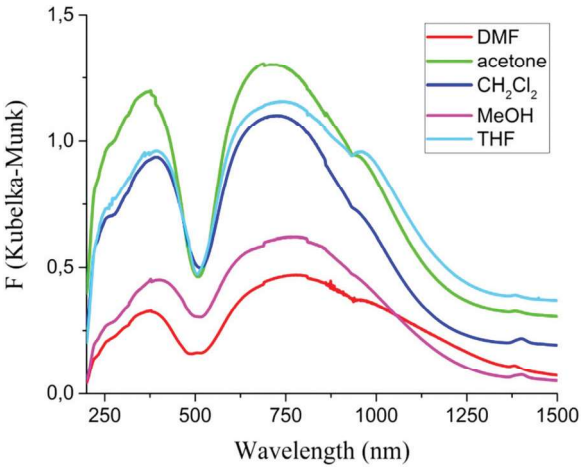

Fig. 10 Solid-state UV-vis spectra of **(Me_2NH_2)[CFA-13](solvent)** at room temperature.

sitions. The absorption bands at 715–750 nm can be assigned to the d–d transitions of Cu(II) centres. The obtained results are in good agreement with the literature data for HKUST-1, which also contains Cu(II) paddle-wheel units and shows similar absorption bands.[24]

Conclusions

The work reported here describes the synthesis and characterisation of the mixed-valent perfluorinated metal–organic framework **(Me_2NH_2)[CFA-13]** assembled from two types of secondary building units. Besides novel trinuclear $[Cu^{I}_3(pz)_4]^-$ coordination units, described here for the first time, the network also exhibits Cu(II) paddle-wheel SBUs. The framework crystallizes in the monoclinic crystal system within the space group $P2_1/n$ (no. 14) and features channels with a limiting diameter of 3.07 Å. Due to a negative charge of the lattice, the pores of the as-synthesized framework are occupied by dimethylammonium cations, which can be readily exchanged with K^+ or Cs^+ ions. **(Me_2NH_2)[CFA-13]** framework is permanently porous after solvent removal, as shown by CO_2 sorption measurements. The framework shows selective binding of reactive gas molecules such as CO and NH_3 based on the presence of different active Cu centres. Thus, linearly coordinated Cu(I) sites within the trinuclear $[Cu^{I}_3(pz)_4]^-$ SBUs selectively bind CO molecules with an isosteric heat of adsorption of up to 47 kJ mol^{-1}. Cu(II) paddle-wheel units, in contrast, show selective binding of NH_3 molecules. Moreover, **CFA-13** shows pronounced photoluminescence properties and offers the possibility to exchange the interchannel cations. Owing to these special features, **CFA-13** represents an interesting example of a bifunctional framework which might be interesting for applications such as sensing or development of new photoluminescent materials. Incorporation of a perfluorinated ligand represents a further advantage of this material, as it should result in higher chemical- and photostability of the framework.

Experimental

Materials and general methods

All starting materials were of analytical grade and used as obtained from commercial sources without further purification. Thermogravimetric analysis (TGA) was performed with a TGA Q500 analyser in the temperature range of 25–600 °C in a flowing nitrogen gas at a heating rate of 5 K min^{-1}. Fourier transform infrared (FTIR) spectra were recorded with an ATR unit in the range of 4000–400 cm^{-1} on a Bruker Equinox 55 FT-IR spectrometer. Diffuse reflectance infrared Fourier-transformed (DRIFT) spectra were recorded with the same instrument equipped with a Harrick Praying Mantis reaction chamber. Energy-dispersive X-ray spectroscopy (EDX) was performed with a Philips XL-30 scanning electron microscope. Ambient temperature X-ray powder diffraction (XRPD) patterns were recorded on a Seifert XRD 3003 TT diffractometer equipped with a Meteor1D detector operated at 40 kV, 40 mA, Cu Kα (λ = 1.54178 Å) with a scan speed of 1 s per step and a step size of 0.02° in 2θ. Variable temperature X-ray powder diffraction (VTXRPD) measurements were collected in the 2θ range of 5–60° with 0.02° steps with a Empyrean (PANalytical) Diffractometer equipped with a Bragg-Brentano^{HD} mirror, a PIXcel^{3D} 2 × 2 detector and a XRK 900 Reactor chamber (Anton Paar). The patterns were recorded in a temperature range from 25 to 400 °C, in the 5–60° 2θ range, with one step per 0.4 s, and an angular step width of 0.02° in 2θ. Temperature program between measurements: heating rate (0.5 $°Cs^{-1}$), then 10 min isothermal. Adsorption isotherms with CO_2 at 273 K (ice/water bath) for the determination of BET surface areas were measured in the relative pressure range 0.0001–0.03 with a Quantachrome NOVA 2000 Series instrument. CO_2 at 194.7 K, CO and O_2 sorption isotherms were measured with a BELSORP-max instrument combined with a BELCryo system. Prior to measurements, the as–synthesized **(Me_2NH_2)[CFA-13](DMF)** sample was heated at 150 °C for 1 h, other samples were heated at 100 °C for 2 h in high vacuum to remove the occluded solvent molecules. Temperature programmed pulse chemisorption measurements were performed using a BelCat-B catalyst analyzer (Bel Japan, Inc.) equipped with a thermal conductivity detector and a coupled mass spectrometer (OmniStar GSD 320, Pfeiffer Vacuum). The volume of the pulse loop was 0.920 mL, the gas flow rate was set to 30 mL min^{-1}. The sample (6.2 mg) was placed between two plugs of superfine quartz wool in a quartz glass reactor. Prior to pulse measurements, the sample was pretreated by heating up to 120 °C (furnace temperature) for 20 minutes at this temperature in He flow. After the pretreatment, 3.99% NH_3 in helium was pulsed at 100 °C to a helium carrier gas stream (99.999%) to titrate the amount of active sites. The results were evaluated with the ChemMaster program (BEL Japan, Inc., version 1.4.0). The adsorbed gas amounts are given in cm^3 g^{-1} [STP], where

STP = 101.3 kPa and 273.15 K. Luminescence spectra were acquired using a spectrofluorimeter (FS920, Edinburgh Instruments) equipped with a TMS300 monochromator, an S900 single photon photomultiplier, and a Xe 900 450 W xenon arc lamp at room temperature. The excitation and emission spectra were corrected for the wavelength-dependent lamp intensity and detector response, respectively.

Synthesis of $(Me_2NH_2)[Cu^I_3Cu^{II}_2(tfpc)_4\cdot 3DMF]\cdot 2.25DMF$

A mixture of copper nitrate trihydrate (24 mg, 0.1 mmol) and H_2-tfpc (25 mg, 0.1 mmol) was dissolved in 2 mL DMF and the solution was placed in a glass tube (10 mL). The tube was closed and heated at 120 °C for 3 days and then cooled to room temperature. The precipitate was filtered and washed with DMF. Yield: 23 mg (66%). IR (ν(cm^{-1})): 2935; 1657; 1624; 1551; 1498; 1437; 1406; 1385; 1250; 1227; 1124; 1100; 1061; 1018; 824; 809; 676; 660; 525; 488; 405. The IR-spectra of **(Me_2NH_2)[CFA-13](DMF)** are shown in ESI (S11 and S12†).

General synthesis procedure for $M[Cu^I_3Cu^{II}_2(tfpc)_4]$ ($M = K^+$, Cs^+)

(Me_2NH_2)[CFA-13](DMF) (30 mg, 0.0173 mmol) was stirred at 50 °C for 1 h in a solution of the corresponding metal nitrate (0.35 mmol) in DMF (1.35 mL) and H_2O (0.4 mL). The excess solvent was decanted and replaced by fresh metal nitrate solution. The exchange procedure was repeated five times. Finally, the precipitate was filtered, washed with water (3 × 2 mL) and DMF (3 × 2 mL). The Cu/M molar ratio of the product was determined by energy dispersive X-ray spectroscopy.

Solvent exchange procedure for (Me_2NH_2)[CFA-13](solvent) (solvents: CH_2Cl_2, EtOH, MeOH, acetone, THF)

(Me_2NH_2)[CFA-13](DMF) (50 mg, 0.03 mmol) was placed in a Soxhlet extractor and refluxed with 60 ml of the corresponding solvent (CH_2Cl_2, EtOH, MeOH, acetone or THF) under nitrogen atmosphere. After 12 h, the solvent was refreshed and refluxed for further 12 h. Finally, the sample was dried under vacuum at room temperature.

Single-crystal X-ray crystallography

X-ray data for the single crystal structure of **$(Me_2NH_2)[Cu^I_3Cu^{II}_2(tfpc)_4\cdot 3DMF]\cdot 2.25DMF$** were collected on a Bruker D8 Venture diffractometer. Intensity measurements were performed using monochromated (doubly curved silicon crystal) MoKα radiation (0.71073 Å) from a sealed microfocus tube. Generator settings were 50 kV, 1 mA. Data collection temperature was −173 °C. APEX3 software was used for preliminary determination of the unit cell.[25] Determination of integrated intensities and unit cell refinement were performed using SAINT.[26] The structure was solved and refined using the Bruker SHELXTL Software Package[27] and refined using SHELXL.[27,28] Selected crystal data and details of the structure refinement for **$(Me_2NH_2)[Cu^I_3Cu^{II}_2(tfpc)_4\cdot 3DMF]\cdot 2.25DMF$** are provided in Table 1. Non-hydrogen atoms were refined with anisotropic temperature parameters. The hydrogen atoms were positioned geometrically and refined using a riding model. Complete crystallographic data for the structure reported in this paper have been deposited in the CIF format with the Cambridge Crystallographic Data Center, 12 Union Road, Cambridge CB21EZ, UK as supplementary publication no. CCDC 1559842.†

Table 1 Crystal data and structure refinement of $(Me_2NH_2)[Cu^I_3Cu^{II}_2(tfpc)_4\cdot 3DMF]\cdot 2.25DMF$

Compound	$(Me_2NH_2)[Cu^I_3Cu^{II}_2(tfpc)_4\cdot 3DMF]\cdot 2.25DMF$
Empirical formula	$C_{41.75}H_{44.75}Cu_5F_{24}N_{14.25}O_{13.25}$
Formula	$(C_2H_8N)[Cu^I_3Cu^{II}_2(C_{24}F_{24}N_8O_8)\cdot 3(C_3H_7NO)]\cdot 2.25(C_3H_7NO)$
M_r/g mol^{-1}	1731.87
T/K	100
Wavelength/Å	0.71073
Crystal system	Monoclinic
Space group	$P2_1/n$ (no. 14)
a/Å	22.3887(19)
b/Å	13.6888(8)
c/Å	21.1804(13)
β/°	90.495(3)
V/Å^3	6491.0(8)
Z	4
D_c/g cm^{-3}	1.772
μ/mm^{-1}	1.747
F(000)	3448
θ range/°	2.350 to 25.056
Refls. collected	89 118
Refls. unique	11 486
R(int)	0.1025
GooF	1.123
R_1 ($I > 2\sigma(I)$)[a]	0.0548
wR_2 (all data)[b]	0.1673
Largest diff. peak and hole/Å^{-3}	0.841 and −0.607

[a] $R_1 = \sum||F_o| - |F_c||/\sum|F_o|$. [b] $wR_2 = \sum[w(F_o^2 - F_c^2)2]/\sum[w(F_o^2)2]^{1/2}$.

Conflicts of interest

There are no conflicts to declare.

Acknowledgements

Financial support by the DFG (Priority Program SPP 1362 "Porous Metal–Organic Frameworks") is gratefully acknowledged.

Notes and references

1 (*a*) J. P. Zhang and S. Kitagawa, *J. Am. Chem. Soc.*, 2008, **130**, 907–917; (*b*) M. Grzywa, C. Geßner, D. Denysenko, B. Bredenkötter, F. Gschwind, K. M. Fromm, W. Nitek, E. Klemm and D. Volkmer, *Dalton Trans.*, 2013, **42**, 6909–6921; (*c*) C. E. Kivi and D. Song, *Dalton Trans.*, 2016, **45**, 17087–17090.

2 (*a*) W.-Y. Gao, R. Cai, T. Pham, K. A. Forrest, A. Hogan, P. Nugent, K. Williams, L. Wojtas, R. Luebke, Ł. J. Weseliński, M. J. Zaworotko, B. Space, Y.-S. Chen,

M. Eddaoudi, X. Shi and S. Ma, *Chem. Mater.*, 2015, **27**, 2144–2151; (*b*) W. Long, W. Qiu, C. Guo, C. Li, L. Song, G. Bai, G. Zhang and H. He, *Molecules*, 2015, **20**, 21178–21192; (*c*) N. Zhu, D. Sensharma, P. Wix, M. J. Lennox, T. Düren, W.-Y. Wong and W. Schmitt, *Eur. J. Inorg. Chem.*, 2016, 1939–1943; (*d*) M. Eddaoudi, J. Kim, J. B. Wachter, H. K. Chae, M. O'Keeffe and O. M. Yaghi, *J. Am. Chem. Soc.*, 2001, **123**, 4368–4369.

3 M. Grzywa, B. Bredenkötter, D. Denysenko, S. Spirkl, W. Nitek and D. Volkmer, *Z. Anorg. Allg. Chem.*, 2013, **639**(8–9), 1461–1471.

4 (*a*) L. Hou, W.-J. Shi, Y.-Y. Wang, H.-H. Wang, L. Cui, P.-X. Chen and Q.-Z. Shi, *Inorg. Chem.*, 2011, **50**, 261–270; (*b*) J.-X. Zhang, J. He, Y.-G. Yin, M.-H. Hu, D. Li and X.-C. Huang, *Inorg. Chem.*, 2008, **47**, 3471–3473; S.-Z. Zhan, M. Li, S. W. Ng and D. Li, *Chem. – Eur. J.*, 2013, **19**, 10217–10225.

5 M. Grzywa, D. Denysenko, A. Schaller, A. Kalytta-Mewes and D. Volkmer, *CrystEngComm*, 2016, **18**, 7883–7893.

6 J.-H. Wang, M. Li and D. Li, *Chem. – Eur. J.*, 2014, **20**, 12004–12008.

7 S. S.-Y. Chui, S. M.-F. Lo, J. P. H. Charmant, A. G. Orpen and I. D. Williams, *Science*, 1999, **283**, 1148–1150.

8 E. Borfecchia, S. Maurelli, D. Gianolio, E. Groppo, M. Chiesa, F. Bonino and C. Lamberti, *J. Phys. Chem. C*, 2012, **116**, 19839–19850.

9 V. K. Peterson, Y. Liu, C. M. Brown and C. J. Kepert, *J. Am. Chem. Soc.*, 2006, **128**, 15578–15579.

10 H. Yamagiwa, S. Sato, T. Fukawa, T. Ikehara, R. Maeda, T. Mihara and M. Kimura, *Sci. Rep.*, 2014, **4**, 6247.

11 K. Schlichte, T. Kratzke and S. Kaskel, *Microporous Mesoporous Mater.*, 2004, **73**, 81–88.

12 A. A. Talin, A. Centrone, A. C. Ford, M. E. Foster, V. Stavila, P. Haney, R. A. Kinney, V. Szalai, F. E. Gabaly, H. P. Yoon, F. Léonard and M. D. Allendorf, *Science*, 2014, (6166), 66–69.

13 (*a*) C. Petit, L. Huang, J. Jagiello, J. Kenvin, K. E. Gubbins and T. J. Bandosz, *Langmuir*, 2011, **27**, 13043–13051; (*b*) C. Petit, B. Mendoza and T. J. Bandosz, *Langmuir*, 2010, **26**, 15302–15309; (*c*) G. W. Peterson, G. W. Wagner, A. Balboa, J. Mahle, T. Sawell and C. J. Karwacki, *J. Phys. Chem. C*, 2009, **113**, 13906–13917.

14 S. Chaemchuen, N. A. Kabir, K. Zhou and F. Verpoort, *Chem. Soc. Rev.*, 2013, **42**, 9304–9332.

15 J. R. Karra and K. S. Walton, *Langmuir*, 2008, **24**, 8620–8626.

16 I. I. Gerus, R. X. Mironetz, I. S. Kondratov, A. V. Bezdudny, Y. V. Dmytriv, O. V. Shishkin, V. S. Starova, O. A. Zaporozhets, A. A. Tolmachev and P. K. Mykhailiuk, *J. Org. Chem.*, 2012, **77**, 47–56.

17 (*a*) P. Schmieder, D. Denysenko, M. Grzywa and D. Volkmer, *Dalton Trans.*, 2016, **45**, 13853–13862; (*b*) M. Grzywa, D. Denysenko, A. Schaller, A. Kalytta-Mewes and D. Volkmer, *CrystEngComm*, 2016, **18**, 7883–7893.

18 M. K. Ehlert, A. Storr, D. A. Summers and R. C. Thompson, *Can. J. Chem.*, 1997, **75**, 491–498.

19 (*a*) M. Melník and M. Dunaj-Jurčo, *Inorg. Chim. Acta*, 1984, **86**, 185–190; (*b*) C. Bronner, S. A. Baudron and M. W. Hosseini, *Inorg. Chem.*, 2010, **49**, 8659–8661; (*c*) A. B. Lago, R. Carballo, S. Rodríguez-Hermida and E. M. Vázquez-López, *Cryst. Growth Des.*, 2014, **14**, 3096–3109; (*d*) B. A. Blight, A. F. Stewart, N. Wang, J.-S. Lu and S. Wang, *Inorg. Chem.*, 2012, **51**, 778–780; (*e*) D. L. Reger, A. Debreczeni, B. Reinecke, V. Rassolov and M. D. Smith, *Inorg. Chem.*, 2009, **48**, 8911–8924.

20 (*a*) A. Spek, *J. Appl. Crystallogr.*, 2003, **36**, 7–13; (*b*) A. L. Spek, *Acta Crystallogr., Sect. C: Cryst. Struct. Commun.*, 2015, **71**, 9–18.

21 W. M. Haynes, *Handbook of Chemistry and Physics*, CRC Press, Cleveland, 2013.

22 H. V. R. Dias and H.-L. Lu, *Inorg. Chem.*, 1995, **34**, 5380–5382.

23 (*a*) N. Armaroli, G. Accorsi, F. Cardinali and A. Listorti, in *Curr Chem*, ed. V. Balzani and S. Campagna, Springer-Verlag, Berlin Heidelberg, Germany, 2007, vol. 280, pp. 69–115; (*b*) P. C. Ford, W. Cariati and J. Bourassa, *Chem. Rev.*, 1999, **99**, 3625–3647.

24 (*a*) C. Prestipino, L. Regli, J. G. Vitillo, F. Bonino, A. Damin, C. Lamberti, A. Zeccina, P. L. Solari, K. O. Kongshaug and S. Bordiga, *Chem. Mater.*, 2006, **18**, 1337–1346; (*b*) H. K. Kim, W. S. Yun, M.-B. Kim, J. Y. Kim, Y.-S. Bae, J. Lee and N. C. Jeong, *J. Am. Chem. Soc.*, 2015, **137**, 10009–10015.

25 *APEX3 Version 2016.9 ed*, Bruker AXS Inc., 2016.

26 *SAINT Version 8.37A ed*, Bruker AXS Inc., 2015.

27 G. M. Sheldrick, XL Version 2013/3, *Acta Crystallogr., Sect. A: Fundam. Crystallogr.*, 2008, **64**, 112.

28 G. M. Sheldrick, *Acta Crystallogr., Sect. C: Cryst. Struct. Commun.*, 2015, **71**, 3–8.